Chapter 8

ELECTRON BEAMS: PHYSICAL AND CLINICAL ASPECTS

W. STRYDOM
Department of Medical Physics,
Medical University of Southern Africa,
Pretoria, South Africa

W. PARKER, M. OLIVARES
Department of Medical Physics,
McGill University Health Centre,
Montreal, Quebec, Canada

8.1. CENTRAL AXIS DEPTH DOSE DISTRIBUTIONS IN WATER

Megavoltage electron beams represent an important treatment modality in modern radiotherapy, often providing a unique option in the treatment of superficial tumours (less than 5 cm deep). Electrons have been used in radiotherapy since the early 1950s, first produced by betatrons and then by microtrons and linacs. Modern high energy linacs typically provide, in addition to two megavoltage photon energies, several electron beam energies in the range from 4 to 22 MeV.

8.1.1. General shape of the depth dose curve

The general shape of the central axis depth dose curve for electron beams differs from that of photon beams (see Fig. 8.1). Figure 8.1(a) shows depth doses for various electron beam energies and Fig. 8.1(b) shows depth doses for 6 and 15 MV X ray beams.

Typically, the electron beam central axis depth dose curve exhibits a high surface dose (compared with megavoltage photon beams), and the dose then builds up to a maximum at a certain depth referred to as the electron beam depth of dose maximum z_{max}. Beyond z_{max} the dose drops off rapidly and levels off at a small low level dose component referred to as the bremsstrahlung tail. These features offer a distinct clinical advantage over the conventional X ray modalities in the treatment of superficial tumours.

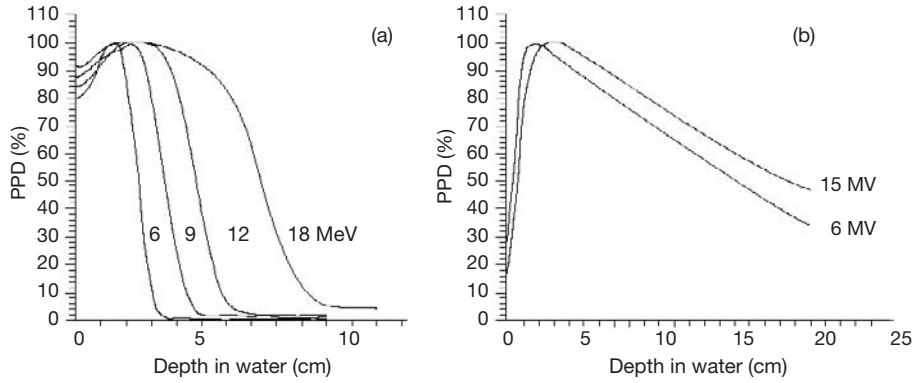

FIG. 8.1. Typical central axis PDD curves in water for a 10 × 10 cm² field size and an SSD of 100 cm for (a) electron beams with energies of 6, 9, 12 and 18 MeV and (b) photon beams with energies of 6 and 15 MV.

A typical high energy linac may produce electron beams with discrete energies in the range from 4 to 25 MeV.

Electron beams can be considered almost monoenergetic as they leave the accelerator; however, as the electron beam passes through the accelerator exit window, scattering foils, monitor chambers, collimators and air, the electrons interact with these structures, resulting in:

- A broadening of the beam's electron energy spectrum;
- Bremsstrahlung production contributing to the bremsstrahlung tail in the electron beam percentage depth dose (PDD) distribution.

On initial contact with the patient, the clinical electron beam has an incident mean energy $\bar{E}_0$ that is lower than the electron energy inside the accelerator.

The ratio of the dose at a given point on the central axis of an electron beam to the maximum dose on the central axis multiplied by 100 is the PDD, which is normally measured for the nominal treatment distance (i.e. the distance between the accelerator exit window and the patient's skin) and depends on field size and electron beam energy.

8.1.2. Electron interactions with an absorbing medium

As electrons travel through a medium, they interact with atoms by a variety of Coulomb force interactions that may be classified as follows:

- Inelastic collisions with atomic electrons, resulting in ionization and excitation of atoms and termed collisional or ionizational loss;
- Elastic collisions with atomic nuclei, resulting in elastic scattering that is characterized by a change in direction but no energy loss;
- Inelastic collisions with atomic nuclei, resulting in bremsstrahlung production and termed radiative loss;
- Elastic collisions with atomic electrons.

The kinetic energy of electrons is lost in inelastic collisions that produce ionization or is converted to other forms of energy, such as photon energy or excitation energy. In elastic collisions kinetic energy is not lost; however, the electron's direction may be changed or the energy may be redistributed among the particles emerging from the collision.

The typical energy loss for a therapy electron beam, averaged over its entire range, is about 2 MeV/cm in water and water-like tissues.

The rate of energy loss for collisional interactions depends on the electron energy and on the electron density of the medium. The rate of energy loss per gram per square centimetre, $MeV \cdot g^{-1} \cdot cm^{-2}$ (called the mass stopping power), is greater for low atomic number materials than for high atomic number materials. This is because high atomic number materials have fewer electrons per gram than lower atomic number materials and, moreover, high atomic number materials have a larger number of tightly bound electrons that are not available for this type of interaction.

The rate of energy loss for radiative interactions (bremsstrahlung) is approximately proportional to the electron energy and to the square of the atomic number of the absorber. This means that X ray production through radiative losses is more efficient for higher energy electrons and higher atomic number materials.

When a beam of electrons passes through a medium the electrons suffer multiple scattering, due to Coulomb force interactions between the incident electrons and predominantly the nuclei of the medium. The electrons will therefore acquire velocity components and displacements transverse to their original direction of motion. As the electron beam traverses the patient, its mean energy decreases and its angular spread increases.

The scattering power of electrons varies approximately as the square of the atomic number and inversely as the square of the kinetic energy. For this reason high atomic number materials are used in the construction of scattering foils used for the production of clinical electron beams in a linac. The scattering power variations in heterogeneous tissues are also responsible for the production of local hot and cold spots.

8.1.3. Inverse square law (virtual source position)

In contrast to a photon beam, which has a distinct focus located at the accelerator X ray target, an electron beam appears to originate from a point in space that does not coincide with the scattering foil or the accelerator exit window. The term 'virtual source position' was introduced to indicate the virtual location of the electron source.

The effective source to surface distance (SSD) for electron beams (SSD_{eff}) is defined as the distance from the virtual source position to the point of the nominal SSD (usually the isocentre of the linac). The inverse square law may be used for small SSD differences from the nominal SSD to make corrections to the absorbed dose for variations in air gaps between the patient surface and the applicator.

There are various methods to determine the SSD_{eff}. One commonly used method consists of measuring the dose at various distances from the electron applicator by varying the gap between the phantom surface and the applicator (with gaps ranging from 0 to 15 cm). In this method, doses are measured in a phantom at the depth of maximum dose z_{max}, with the phantom first in contact with the applicator (zero gap) and then at various distances g from the applicator. Suppose I_0 is the dose with zero gap ($g = 0$) and I_g is the dose with gap distance g. It follows then from the inverse square law that:

$$\frac{I_0}{I_g} = \left(\frac{\mathrm{SSD}_{\mathrm{eff}} + z_{\max} + g}{\mathrm{SSD}_{\mathrm{eff}} + z_{\max}} \right)^2 \tag{8.1}$$

or

$$\sqrt{\frac{I_0}{I_g}} = \frac{g}{\mathrm{SSD}_{\mathrm{eff}} + z_{\max}} + 1 \tag{8.2}$$

A plot of $\sqrt{I_0 / I_g}$ against the gap distance g will give a straight line with a slope of:

$$\frac{1}{\mathrm{SSD}_{\mathrm{eff}} + z_{\max}}$$

and the SSD_{eff} will then be given by:

$$\mathrm{SSD}_{\mathrm{eff}} = \frac{1}{\mathrm{slope}} - z_{\max} \tag{8.3}$$

Although the effective SSD is obtained from measurements at z_{max}, its value does not change with the depth of measurement. However, the effective SSD changes with beam energy, and has to be measured for all energies available in the clinic.

8.1.4. Range concept

A charged particle such as an electron is surrounded by its Coulomb electric field and will therefore interact with one or more electrons or with the nucleus of practically every atom it encounters. Most of these interactions individually transfer only minute fractions of the incident particle's kinetic energy, and it is convenient to think of the particle as losing its kinetic energy gradually and continuously in a process often referred to as the continuous slowing down approximation (CSDA).

The path length of a single electron is the total distance travelled along its actual trajectory until the electron comes to rest, regardless of the direction of movement. The projected path range is the sum of individual path lengths projected on to the incident beam direction (i.e. the central axis). The CSDA range (or the mean path length) for an electron of initial kinetic energy E_0 can be found by integrating the reciprocal of the total stopping power:

$$R_{CSDA} = \int_0^{E_0} \left[\frac{S(E)}{\rho} \right]_{tot}^{-1} dE \tag{8.4}$$

The CSDA range is purely a calculated quantity that represents the mean path length along the electron's trajectory and not the depth of penetration in a defined direction. The CSDA range for electrons in air and water is given in Table 8.1 for various electron kinetic energies.

The following two concepts of range are also defined for electron beams: maximum range and practical range.

The maximum range R_{max} (cm or g/cm^2) is defined as the depth at which extrapolation of the tail of the central axis depth dose curve meets the bremsstrahlung background, as shown in Fig. 8.2. It is the largest penetration depth of electrons in the absorbing medium. The maximum range has the drawback of not giving a well defined measurement point.

The practical range R_p (cm or g/cm^2) is defined as the depth at which the tangent plotted through the steepest section of the electron depth dose curve intersects with the extrapolation line of the background due to bremsstrahlung, as shown in Fig. 8.2.

TABLE 8.1. CSDA RANGES IN AIR AND WATER FOR VARIOUS ELECTRON ENERGIES

Electron energy (MeV)	CSDA range in air (g/cm^2)	CSDA range in water (g/cm^2)
6	3.255	3.052
7	3.756	3.545
8	4.246	4.030
9	4.724	4.506
10	5.192	4.975
20	9.447	9.320
30	13.150	13.170

The depths R_{90} and R_{50} (cm or g/cm^2) are defined as depths on the electron PDD curve at which the PDDs beyond z_{max} attain values of 90% and 50%, respectively.

The depth R_q (cm or g/cm^2) is defined as the depth where the tangent through the dose inflection point intersects the maximum dose level, as shown in Fig. 8.2.

It is evident that the CSDA range is of marginal usefulness in characterizing the depth of penetration of electrons into an absorbing medium.

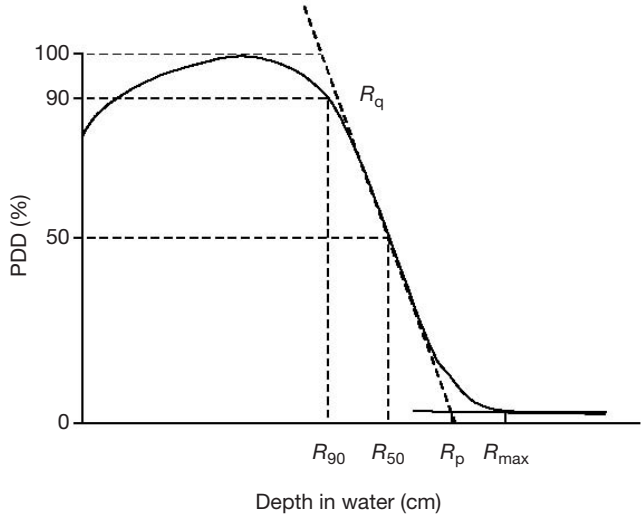

FIG. 8.2. Typical electron beam PDD curve illustrating the definition of R_q, R_p, R_{max}, R_{50} and R_{90}.

Scattering effects, predominantly between the incident electrons and nuclei of the absorbing medium, cause electrons to follow very tortuous paths, resulting in large variations in the actual path of electrons in the absorbing medium.

8.1.5. Buildup region (depths between the surface and z_{max} (i.e. $0 \leq z \leq z_{max}$))

The dose buildup in electron beams is much less pronounced than that of megavoltage photon beams and results from the scattering interactions that the electrons experience with atoms of the absorber. Upon entry into the medium (e.g. water), the electron paths are approximately parallel. With depth their paths become more oblique with regard to the original direction, due to multiple scattering, resulting in an increase in electron fluence along the beam central axis.

In the collision process between electrons and atomic electrons, it is possible that the kinetic energy acquired by the ejected electron is large enough (hard collision) to cause further ionization. In such a case, these electrons are referred to as secondary electrons or δ rays, and they also contribute to the buildup of dose.

As seen in Fig. 8.1, the surface dose of electron beams (in the range from 75% to 95%) is much higher than the surface dose for photon beams, and the rate at which the dose increases from the surface to z_{max} is therefore less pronounced for electron beams than for photon beams.

Unlike in photon beams, the per cent surface dose for electron beams increases with electron energy. This can be explained by the nature of electron scatter. At lower energies, electrons are scattered more easily and through larger angles. This causes the dose to build up more rapidly and over a shorter distance, as shown in Fig. 8.3. The ratio of surface dose to maximum dose is therefore lower for lower energy electrons than for higher energy electrons.

In contrast to the behaviour of megavoltage photon beams, the depth of maximum dose in electron beams z_{max} does not follow a specific trend with electron beam energy; rather, it is a result of the machine design and accessories used.

8.1.6. Dose distribution beyond z_{max} ($z > z_{max}$)

Scattering and continuous energy loss by electrons are the two processes responsible for the sharp drop-off in the electron dose at depths beyond z_{max}.

Bremsstrahlung produced in the head of the accelerator, in the air between the accelerator window and the patient, and in the irradiated medium is responsible for the tail in the depth dose curve.

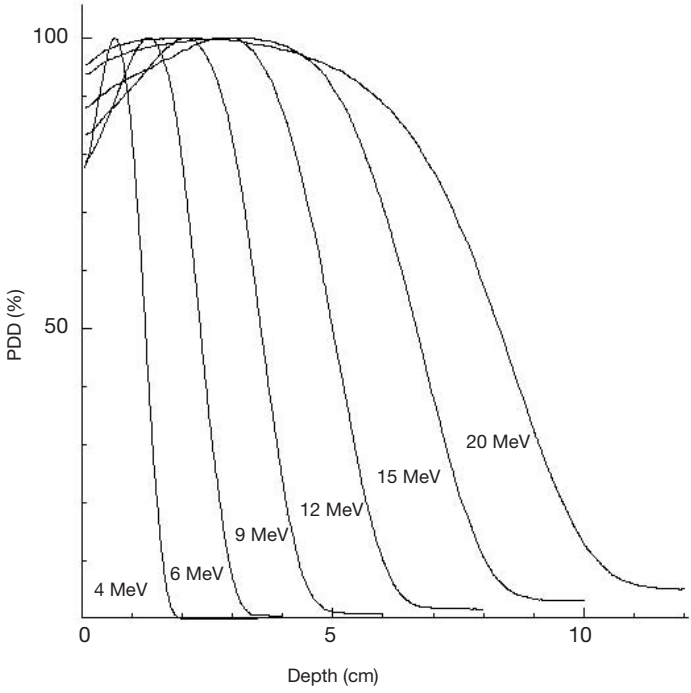

FIG. 8.3. Central axis PDD curves for a family of electron beams from a high energy linac. All curves are normalized to 100% at z_{max}.

The range of electrons increases with increasing electron energy. The electron dose gradient is defined as follows:

$$G = R_p/(R_p - R_q)$$

The dose gradient for lower electron energies is steeper than that for higher electron energies, since the lower energy electrons are scattered at a greater angle away from their initial directions. The stopping powers at low and high energy also affect the dose gradient.

The bremsstrahlung contamination (e.g. the tail sections of Fig. 8.1(a)) depends on electron beam energy and is typically less than 1% for 4 MeV and less than 4% for 20 MeV electron beams for an accelerator with dual scattering foils.

8.2. DOSIMETRIC PARAMETERS OF ELECTRON BEAMS

8.2.1. Electron beam energy specification

Owing to the complexity of the spectrum, there is no single energy parameter that will fully characterize an electron beam. Several parameters are used to describe a beam, such as the most probable energy $E_{p,0}$ on the phantom surface, the mean energy $\bar{E}_0$ on the phantom surface, and R_{50}, the depth at which the absorbed dose falls to 50% of the maximum dose.

The most probable energy $E_{p,0}$ on the phantom surface is empirically related to the practical range R_p in water as follows:

$$E_{p,0} = 0.22 + 1.09R_p + 0.0025R_p^2 \tag{8.5}$$

where $E_{p,0}$ is in megaelectronvolts and R_p is in centimetres.

The mean electron energy $\bar{E}_0$ at the phantom surface is related to the half-value depth R_{50} as follows:

$$\bar{E}_0 = CR_{50} \tag{8.6}$$

where $C = 2.33$ MeV/cm for water.

The depth R_{50} is the beam quality index in electron beam dosimetry as specified in IAEA TRS 398. R_{50} is calculated from the measured $R_{50,ion}$, the depth at which the ionization curve falls to 50% of its maximum, by:

$$R_{50} = 1.029R_{50,ion} - 0.06 \text{ (g/cm}^2\text{)} \text{ (for } R_{50,ion} \leq 10 \text{ g/cm}^2\text{)} \tag{8.7}$$

$$R_{50} = 1.059R_{50,ion} - 0.37 \text{ (g/cm}^2\text{)} \text{ (for } R_{50,ion} > 10 \text{ g/cm}^2\text{)} \tag{8.8}$$

$\bar{E}_z$, the mean energy at a depth z in a water phantom, is related to the practical range R_p by the Harder equation as follows:

$$\bar{E}_z = \bar{E}_0 (1 - z/R_p) \tag{8.9}$$

8.2.2. Typical depth dose parameters as a function of energy

Some typical values for electron depth dose parameters as a function of energy are shown in Table 8.2. These parameters should be measured for each electron beam before it is put into clinical service.

TABLE 8.2. TYPICAL DEPTH DOSE PARAMETERS OF ELECTRON BEAMS

Energy (MeV)	R_{90} (cm)	R_{80} (cm)	R_{50} (cm)	R_p (cm)	$\bar{E}_0$ (MeV)	Surface dose (%)
6	1.7	1.8	2.2	2.9	5.6	81
8	2.4	2.6	3.0	4.0	7.2	83
10	3.1	3.3	3.9	4.8	9.2	86
12	3.7	4.1	4.8	6.0	11.3	90
15	4.7	5.2	6.1	7.5	14.0	92
18	5.5	5.9	7.3	9.1	17.4	96

8.2.3. Percentage depth dose

Typical central axis PDD curves for various electron beam energies are shown in Fig. 8.3 for a field size of 10×10 cm^2.

When diodes are used in PDD measurements, the diode signal represents the dose directly, because the stopping power ratio water to silicon is essentially independent of electron energy and hence depth.

If an ionization chamber is used in the determination of electron beam depth dose distributions, the measured depth ionization distribution must be converted to a depth dose distribution by using the appropriate stopping power ratios water to air at depths in a phantom. For more information on the ionization chamber measurements see IAEA TRS 398.

8.2.3.1. Percentage depth doses for small electron field sizes

When the distance between the central axis and the field edge is more than the lateral range of scattered electrons, lateral scatter equilibrium exists and the depth dose for a specific electron energy will be essentially independent of the field dimensions, as shown in Fig. 8.4 for field sizes larger than 10×10 cm^2 and an electron energy of 20 MeV.

With decreasing field size the decreasing degree of lateral electronic equilibrium will be present at the central axis, and the depth dose and output factors will show large sensitivity to field shape and size (see also Section 8.3.2), as shown in Fig. 8.4 for a 20 MeV electron beam and field sizes smaller than 10×10 cm^2.

When the length of one side of the electron field decreases to below the R_p value for a given electron energy, the depth of dose maximum decreases and

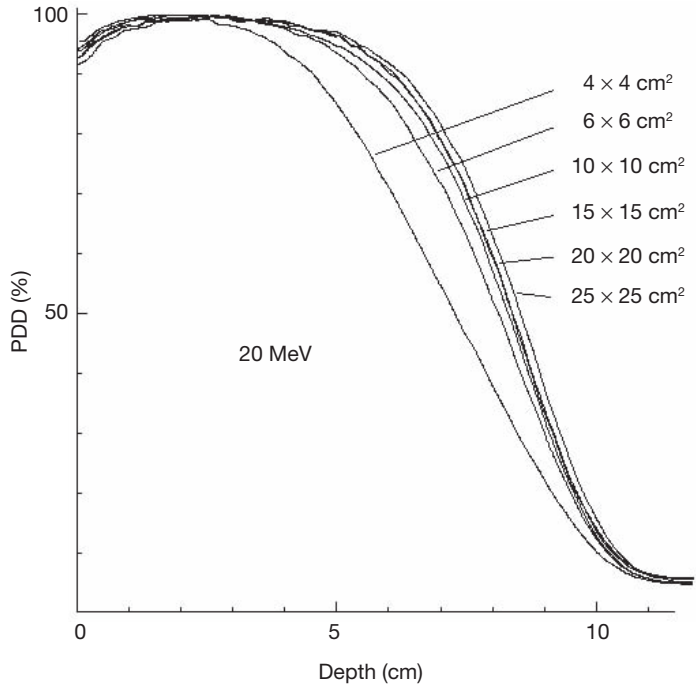

FIG. 8.4. PDD curves for different field sizes for a 20 MeV electron beam from a linac. It is clearly illustrated that for field sizes larger than the practical range of the electron beam (R_p is about 10 cm for this 20 MeV electron beam), the PDD curve remains essentially unchanged.

the relative surface dose increases with decreasing field size. The R_p, on the other hand, is independent of electron beam field size, as also shown in Fig. 8.4, and depends only on electron beam energy.

8.2.3.2. Percentage depth doses for oblique beam incidence

The distributions in Fig. 8.3 are given for normal (perpendicular) beam incidence on the phantom or patient surface. For oblique beam incidences with angles α between the beam central axis and the normal to the phantom or patient surface exceeding 20º, there are significant changes to the PDD characteristics of the electron beam, in contrast to the behaviour observed in photon beams.

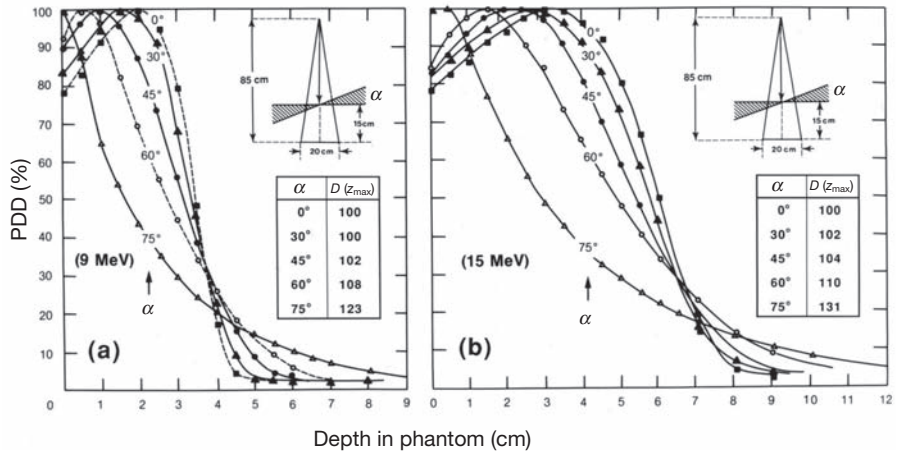

FIG. 8.5. PDD curves for various beam incidences for a (a) 9 MeV and (b) 15 MeV electron beam. $\alpha = 0$ represents normal beam incidence. The inset shows the geometry of the experimental set-up and the doses at z_{max} for various angles α relative to the dose at z_{max} for $\alpha = 0$.

Figure 8.5 illustrates the effect of the beam incidence angle α on PDD distributions. Angle $\alpha = 0$ represents normal incidence. The larger the angle α, the shallower is z_{max} and the larger is the dose at z_{max}. All dose values are normalized to 100% at z_{max} for $\alpha = 0$.

For small angles of incidence α, the slope of the PDD curve decreases and the practical range is essentially unchanged from that for normal beam incidence. When the angle of incidence α exceeds 60º, the PDD looses its characteristic shape and the definition of R_p can no longer be applied. For large angles of incidence, the dose at z_{max} increases significantly. This effect is due to the increased electron fluence through the central axis from the oblique beam angle.

8.2.4. Output factors

An important parameter that determines the electron beam output is the collimator jaw setting. For each electron applicator (cone) there is an associated jaw setting that is generally larger than the field size defined by the applicator (electron beam cone). Such an arrangement minimizes the variation of collimator scatter and therefore the output variation with field size is kept reasonably small. Typical electron applicator sizes are 6×6, 10×10, 15×15, 20×20 and 25×25 cm^2.

The output factor for a given electron energy is the ratio of the dose for any specific field size (applicator size) to the dose for a 10×10 cm^2 reference applicator, both measured at z_{max} in a phantom at an SSD of 100 cm.

The square field defined by the applicator will not adequately shield all normal tissues in most clinical situations. For this reason collimating blocks fabricated from lead or a low melting point alloy are routinely inserted into the end of the applicator to shape the fields. Output factors must also be measured for these irregular fields shaped by cut-outs.

For small field sizes this extra shielding will affect the PDD and the output factors due to lack of lateral scatter. The change in z_{max} as well as changes in the PDDs with small field sizes must be accounted for when measuring output factors.

8.2.5. Therapeutic range R_{90}

The depth of the 90% dose level (R_{90} (cm)) beyond z_{max} is defined as the therapeutic range for electron beam therapy. The R_{90} depth should, if possible, coincide with the distal treatment margin. This depth is approximately given by $E/4$ in centimetres of water, where E is the nominal energy in megaelectron-volts of the electron beam. R_{80} (cm), the depth that corresponds to the 80% PDD beyond z_{max}, is also a frequently used parameter for defining the therapeutic range, and can be approximated by $E/3$ in centimetres of water.

8.2.6. Profiles and off-axis ratios

A typical dose profile for a 6 MeV electron beam and a 25×25 cm^2 field at z_{max} is shown in Fig. 8.6. The off-axis ratio (OAR) relates the dose at any point in a plane perpendicular to the beam direction to the dose on the central axis in that plane. A plot of the OAR against the distance from the central axis is referred to as a dose profile.

8.2.7. Flatness and symmetry

The specification for the flatness of electron beams according to the IEC is given at z_{max} and consists of two requirements:

- The flatness specification requires that the distance between the 90% dose level and the geometrical beam edge should not exceed 10 mm along the major axes and 20 mm along the diagonals;

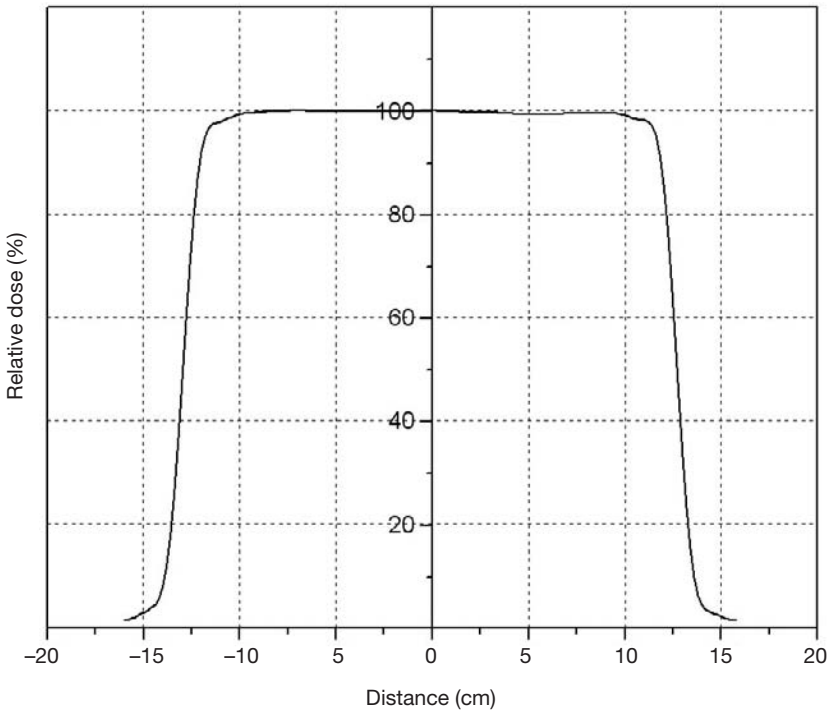

FIG. 8.6. Dose profile at depth z_{max} for a 12 MeV electron beam and 25 × 25 cm^2 field.

- The maximum value of the absorbed dose anywhere within the region bounded by the 90% isodose contour should not exceed 1.05 times the absorbed dose on the axis of the beam at the same depth.

The specification for symmetry of electron beams according to the IEC at $z_{\max}$ is that the cross-beam profile should not differ by more than 3% for any pair of symmetric points with respect to the central ray.

8.3. CLINICAL CONSIDERATIONS IN ELECTRON BEAM THERAPY

8.3.1. Dose specification and reporting

Electron beam therapy is usually applied for the treatment of superficial or subcutaneous disease. Treatments are usually delivered with a single direct

electron field at a nominal SSD of 100 cm. The dose specification for treatment is commonly given at a depth that lies at, or beyond, the distal margin of the disease, and the energy chosen for the treatment depends on the depth of the lesion to be treated.

To maximize healthy tissue sparing beyond the tumour, while at the same time providing relatively homogeneous target coverage, treatments are usually prescribed at either z_{max}, R_{90} or R_{80}. If the treatment dose is specified at either R_{80} or R_{90}, the skin dose will often be higher than the prescription dose. The maximum dose to the patient could be up to 20% higher than the prescribed dose. The maximum dose should therefore always be reported for electron beam therapy.

8.3.2. Small field sizes

For field sizes larger than the practical range of the electron beam, the PDD curve remains constant with increasing field size, since the electrons from the periphery of the field are not scattered sufficiently to contribute to the central axis depth dose. When the field is reduced below that required for lateral scatter equilibrium, the dose rate decreases, z_{max} moves closer to the surface and the PDD curve becomes less steep (see Fig. 8.4). Therefore, for all treatments involving small electron beam field sizes, the beam output as well as the full PDD distribution must be determined for a given patient treatment.

8.3.3. Isodose curves

Isodose curves (see Fig. 8.7) are lines passing through points of equal dose. Isodose curves are usually drawn at regular intervals of absorbed dose and are expressed as a percentage of the dose at a reference point, which is normally taken as the z_{max} point on the beam central axis. As an electron beam penetrates a medium, the beam expands rapidly below the surface, due to scattering. However, the individual spread of the isodose curves varies depending on the isodose level, energy of the beam, field size and beam collimation.

A particular characteristic of electron beam isodose curves is the bulging of the low value curves (<20%) as a direct result of the increase in electron scattering angle with decreasing electron energy. At energies above 15 MeV, electron beams exhibit a lateral constriction of the higher value isodose curves (>80%).

Isodose curves for a 9 and 20 MeV electron beam are shown in Fig. 8.7. The phenomena of bulging and constricting isodose curves are clearly visible.

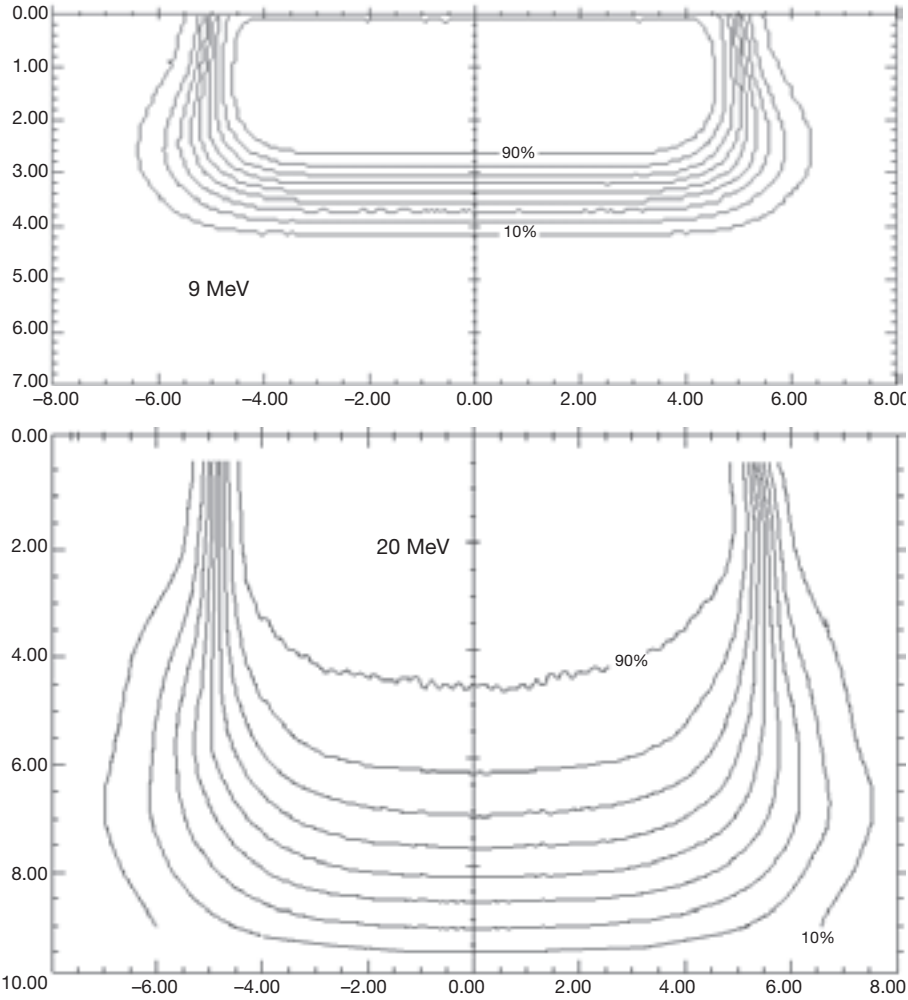

FIG. 8.7. Measured isodose curves for 9 and 20 MeV electron beams. The field size is 10 × 10 cm^2 and SSD = 100 cm. Note the bulging low value isodose lines for both beam energies. The 80% and 90% isodose lines for the 20 MeV beam exhibit a severe lateral constriction. The abscissa and the ordinate represent distance from the central axis and depth in a water phantom, respectively, measured in centimetres.

The term penumbra generally defines the region at the edge of a radiation beam over which the dose rate changes rapidly as a function of distance from the beam central axis. The physical penumbra of an electron beam may be defined as the distance between two specified isodose curves at a specified depth. A penumbra defined in this way is a rapidly varying function of depth.

The ICRU has recommended that the 80% and 20% isodose lines be used in the determination of the physical penumbra, and that the specified depth of measurement be $R_{85}/2$, where R_{85} is the depth of the 85% dose level beyond z_{max} on the electron beam central axis.

The low value isodose lines (e.g. below the 50% isodose line) diverge with increasing air gap between the patient and the end of the applicator (cone), while the high value isodose lines converge towards the central axis. This means that the penumbra will increase if the distance from the applicator increases.

8.3.4. Field shaping

Field shaping for electron beams is always achieved with electron applicators (cones), which may be used alone or in conjunction with shielding blocks or special cut-outs.

8.3.4.1. Electron applicators

Normally the photon beam collimators on the accelerator are too far from the patient to be effective for electron field shaping. After passing through the scattering foil, the electrons scatter sufficiently with the other components of the accelerator head, and in the air between the exit window and the patient, to create a clinically unacceptable penumbra.

Electron beam applicators or cones are usually used to collimate the beam, and are attached to the treatment unit head such that the electron field is defined at distances as small as 5 cm from the patient. Several cones are provided, usually in square field sizes ranging from 5×5 cm^2 to 25×25 cm^2.

8.3.4.2. Shielding and cut-outs

For a more customized field shape, a lead or metal alloy cut-out may be constructed and placed on the applicator as close to the patient as possible. Standard cut-out shapes may be preconstructed and ready for use at the time of treatment. Custom cut-out shapes may also be designed for patient treatment. Field shapes may be determined from conventional or virtual simulation, but are most often prescribed clinically by the physician prior to the first treatment.

The lead thickness required for the shielding of various electron energies with transmissions of 50%, 10% and 5% is given in Table 8.3. As a rule of thumb, simply divide the practical range R_p by 10 to obtain the approximate thickness of lead required for shielding (<5% transmission).

TABLE 8.3. LEAD THICKNESS (mm) REQUIRED FOR VARIOUS TRANSMISSION LEVELS FOR A 12.5 × 12.5 cm^2 ELECTRON FIELD

Transmission (%)	Energy (MeV)						
	6	8	10	12	14	17	20
50	1.2	1.8	2.2	2.6	2.9	3.8	4.4
10	2.1	2.8	3.5	4.1	5.0	7.0	9.0
5	3.0	3.7	4.5	5.6	7.0	8.0	10.0

8.3.4.3. Internal shielding

For certain treatments, such as treatments of the lip, buccal mucosa, eyelids or ear lobes, it may be advantageous to use an internal shield to protect the normal structures beyond the target volume. Care must be taken to consider the dosimetric effects of placing lead shielding directly on the patient's surface. A high dose may inadvertantly be delivered to healthy tissue in contact with the shield owing to electron backscattering from the shield. This dose enhancement can be appreciable and may reach levels of 30–70%, but drops off exponentially with distance from the interface on the entrance side of the beam.

Aluminium or acrylic materials have been used around lead shields to absorb the backscattered electrons. Often, these shields are dipped in wax to form a 1 or 2 mm coating around the lead. This not only protects the patient from the toxic effects of the lead, but also absorbs any scattered electrons, which are usually low in energy.

8.3.4.4. Extended source to surface distance treatments

In clinical situations in which a set-up at the nominal SSD is precluded, an extended SSD might be used, although, as a general rule, such treatments should be avoided unless absolutely necessary.

Extending the SSD typically produces a large change in output, a minimal change in PDD and a significant change in beam penumbra. The beam penumbra can be restored by placing collimation on the skin surface. The inside edge of the skin collimation has to be well within the penumbra cast by the normal treatment collimator. Clinical electron beams are not produced at a single source position in the head of the linac, but rather as an interaction of a pencil beam with the scattering foil and other components.

In general, the inverse square law, as used for photon beams, cannot be applied to electron beams without making a correction.

A virtual source position for electron beams can be determined experimentally as the point in space that appears to be the point source position for the electron beam. An 'effective' SSD, based on the virtual source position, is used when applying the inverse square law to correct for a non-standard SSD.

8.3.5. Irregular surface correction

A frequently encountered situation in electron beam therapy is that where the end of the treatment cone is not parallel to the skin surface of the patient. This could result in an uneven air gap, and corrections would have to be made to the dose distribution to account for the sloping surface. Corrections to isodose lines can be applied on a point by point basis through the use of the following equation:

$$D(\mathrm{SSD}_{\mathrm{eff}} + g, z) = D_0(\mathrm{SSD}_{\mathrm{eff}}, z)\left(\frac{\mathrm{SSD}_{\mathrm{eff}} + z}{\mathrm{SSD}_{\mathrm{eff}} + g + z}\right)^2 \times \mathrm{OF}(\theta, z) \qquad (8.10)$$

where

$\mathrm{SSD}_{\mathrm{eff}}$ is the effective SSD;
g is the air gap;
z is the depth in the patient;
θ is the obliquity angle between the tangent to the skin surface and the beam central axis;
$D_0(\mathrm{SSD}_{\mathrm{eff}}, z)$ is the dose at depth z for a beam incident normally on a flat phantom;
$\mathrm{OF}(\theta, z)$ is a correction factor for the obliquity of the beam that tends to unity for beams of perpendicular incidence. This factor may either be measured or looked up in the literature.

8.3.6. Bolus

Bolus, made of a tissue equivalent material such as wax, is often used in electron beam therapy for the following purposes:

- To increase the surface dose;
- To flatten out irregular surfaces;
- To reduce the electron beam penetration in some parts of the treatment field.

For very superficial lesions, the practical range of even the lowest energy beam available from a linac may be too large to provide adequate healthy tissue sparing beyond the tumour depth. To overcome this problem, a tissue equivalent bolus material of specified thickness is placed on the surface of the patient with the intent to shorten the range of the beam in the patient.

Bolus may also be used to define more precisely the range of the electron beam. The difference between the available electron beam energies from a linac is usually no less than 3 or 4 MeV. If the lower energy is not penetrating enough and the next available energy is too penetrating, bolus may be used with the higher energy beam to fine tune the electron beam range. Bolus can also be used to shape isodose lines to conform to tumour shapes.

Sharp surface irregularities, where the electron beam may be incident tangentially, give rise to a complex dose distribution with hot and cold spots. Tapered bolus around the irregularity may be used to smooth out the surface and reduce the dose inhomogeneity.

Although labour intensive, the use of bolus for electron beam treatments is very practical, since treatment planning software for electron beams is limited and empirical data are normally collected only for standard beam geometries.

The use of computed tomography (CT) for treatment planning enables accurate determination of the tumour shape and depth and the patient contour. If a wax bolus can be constructed such that the total distance from the surface of the bolus to the required treatment depth is constant along the length of the tumour, then the shape of the resulting isodose curves should approximate the shape of the tumour (see Fig. 8.8).

8.3.7. Inhomogeneity corrections

The dose distribution from an electron beam can be greatly affected by the presence of tissue inhomogeneities such as lung or bone. The dose within these inhomogeneities is difficult to calculate or measure, but the effect on the distribution beyond the inhomogeneity is quantifiable.

8.3.7.1. Coefficient of equivalent thickness

The simplest correction for tissue inhomogeneities involves the scaling of the inhomogeneity thickness by its density relative to water, and the determination of a coefficient of equivalent thickness (CET).

The CET of a material is given by its electron density relative to the electron density of water and is essentially equivalent to the mass density of the

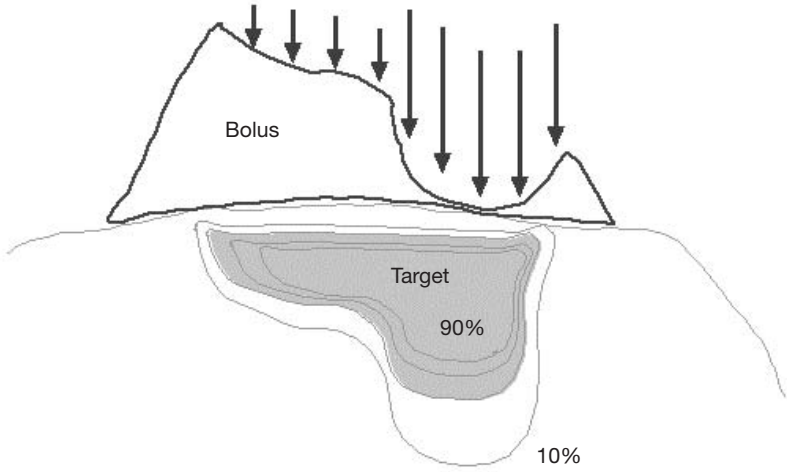

FIG. 8.8. Construction of a custom bolus to conform isodose lines to the shape of the target.

inhomogeneity; for example, lung has an approximate density of 0.25 g/cm^3 and a CET of 0.25. Thus a thickness of 1 cm of lung is equivalent to 0.25 cm of tissue. Solid bone has a CET of approximately 1.6.

The CET can be used to determine an effective depth in water equivalent tissue z_{eff} through the following expression:

$$z_{\text{eff}} = z - t(1 - \text{CET}) \tag{8.11}$$

where z is the actual depth of the point in the patient and t is the thickness of the inhomogeneity.

Figure 8.9 illustrates the effect of a lung inhomogeneity on the PDD curve of an electron beam.

8.3.7.2. Scatter perturbation (edge) effects

If an electron beam strikes the interface between two materials either tangentially or at a large oblique angle, the resulting scatter perturbation will affect the dose distribution at the interface. The lower density material will receive a higher dose, due to the increased scattering of electrons from the higher density side.

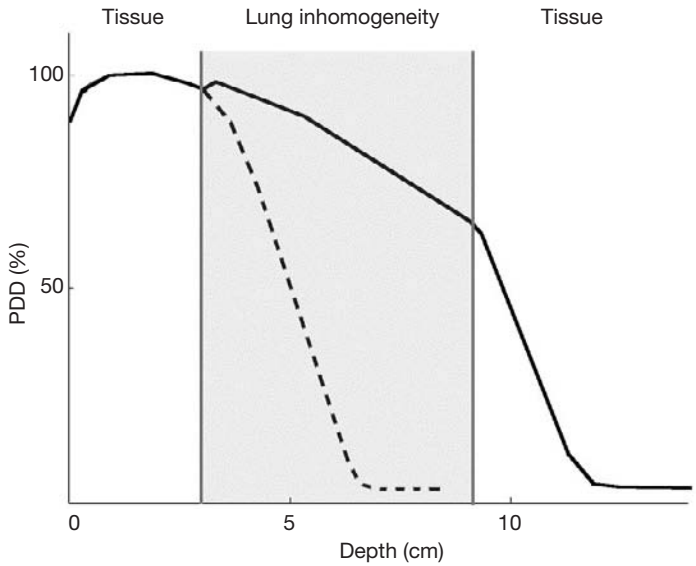

FIG. 8.9. Effect of a 5 cm lung inhomogeneity on a 15 MeV, 10 × 10 cm^2 electron beam PDD. The dashed curve represents the PDD in tissue without the inhomogeneity present.

Edge effects need to be considered in the following situations:

- Inside a patient, at the interfaces between internal structures of different density;
- On the surface of the patient, in regions of sharp surface irregularity;
- On the interface between lead shielding and the surface of the patient, if the shielding is placed superficially on the patient or if it is internal shielding.

The enhancement in dose at the tissue–metal interface is dependent on the beam energy at the interface and on the atomic number of the metal. In the case of a tissue–lead interface, the electron backscatter factor (EBF) is empirically given by:

$$\mathrm{EBF} = 1 + 0.735 e^{-0.052 \bar{E}_{\mathrm{d}}} \tag{8.12}$$

where $\bar{E}_{\mathrm{d}}$ is the average energy of the electrons incident on the interface. This equation, given by Klevenhagen, represents the best fit to the experimental data.

8.3.8. Electron beam combinations

Electron beams may be abutted to adjacent electron fields or to adjacent photon fields.

8.3.8.1. Matched (abutted) electron fields

When abutting electron fields, it is important to take into consideration the dosimetric characteristics of electron beams at depth. The large penumbra and bulging isodose lines make hot spots and cold spots in the target volume practically unavoidable. Contiguous electron beams should be parallel to each other, in order to avoid significant overlapping of the high value isodose curves at depth.

In general, it is best to avoid adjacent electron fields, but if treatment with these fields is absolutely necessary, some basic film dosimetry should be carried out at the junction prior to treatment to verify that no hot or cold spots in dose are present.

8.3.8.2. Matched photon and electron fields

Electron–photon field matching is easier than electron–electron field matching. A distribution for photon fields is usually available from a treatment planning system (TPS), and the location of the electron beam treatment field as well as the associated hot and cold spots can be determined relative to the photon field treatment plan. The matching of electron and photon fields on the skin will produce a hot spot on the photon side of the treatment.

8.3.9. Electron arc therapy

Electron arc therapy is a special radiotherapeutic technique in which a rotational electron beam is used to treat superficial tumour volumes that follow curved surfaces. While the technique is well known and accepted as clinically useful in the treatment of certain tumours, it is not widely used because it is relatively complicated and its physical characteristics are poorly understood. The dose distribution in the target volume depends in a complicated fashion on the electron beam energy, field width, depth of the isocentre, source to axis distance (SAD), patient curvature, tertiary collimation and field shape as defined by the secondary collimator.

The excellent clinical results achieved by the few pioneers in this field during the past two decades have certainly stimulated an increased interest in electron arc therapy, both for curative treatments and for palliation. In fact,

manufacturers of linacs now offer the electron arc therapy mode as one of the standard treatment options. While this option is usually purchased with a new linac, since it is relatively inexpensive, it is rarely used clinically because of the technical difficulties involved.

Two approaches to electron arc therapy have been developed: the simpler is referred to as electron pseudo arc and is based on a series of overlapping stationary electron fields, and the other uses a continuous rotating electron beam. The calculation of dose distributions in electron arc therapy is a complicated procedure and usually cannot be performed reliably with the algorithms used for standard stationary electron beam treatment planning.

The angle β concept offers a semiempirical technique for treatment planning for electron arc therapy. The characteristic angle β for an arbitrary point A on the patient's surface (Fig. 8.10) is measured between the central axes of two rotational electron beams positioned in such a way that at point A the frontal edge of one beam crosses the trailing edge of the other beam.

The angle β is uniquely determined by three treatment parameters: f, the SAD; d_i, the depth of the isocentre; and w, the field width. Electron beams with combinations of d_i and w that give the same characteristic angle β actually exhibit very similar radial PDDs, even though they may differ considerably in individual d_i and w (see Fig. 8.11). Thus the PDDs for rotational electron beams depend only on the electron beam energy and on the characteristic angle β.

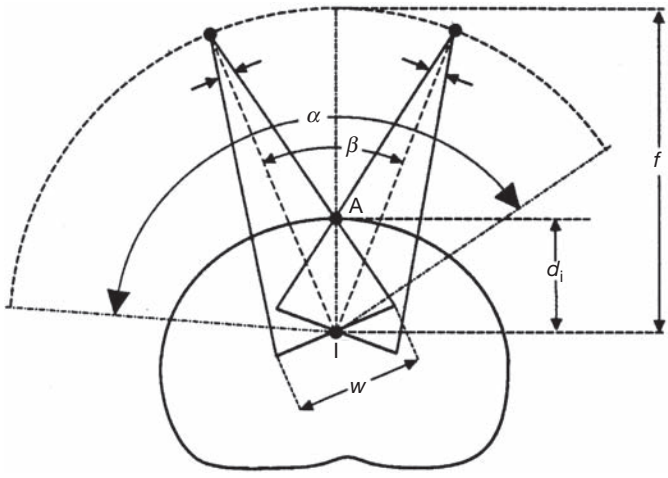

FIG. 8.10. Arc therapy geometry: f is the SAD; d_i is the depth of the isocentre; w is the field width defined at the isocentre; α is the arc angle or the angle of treatment; and β is the characteristic angle for the particular treatment geometry.

Photon contamination is of concern in electron arc therapy, since the photon contribution from all beams is added at the isocentre and the isocentre might be placed on a critical structure. Figure 8.12 shows a comparison between two dose distributions measured with film in a humanoid phantom. Figure 8.12(a) is for a small β of 10º (i.e. a small field width) and clearly exhibits a large photon dose at the isocentre, while Fig. 8.12(b) was taken for a large β of 100º and exhibits a low photon dose at the isocentre. In arc therapy the isocentre bremsstrahlung dose is inversely proportional to the characteristic angle β.

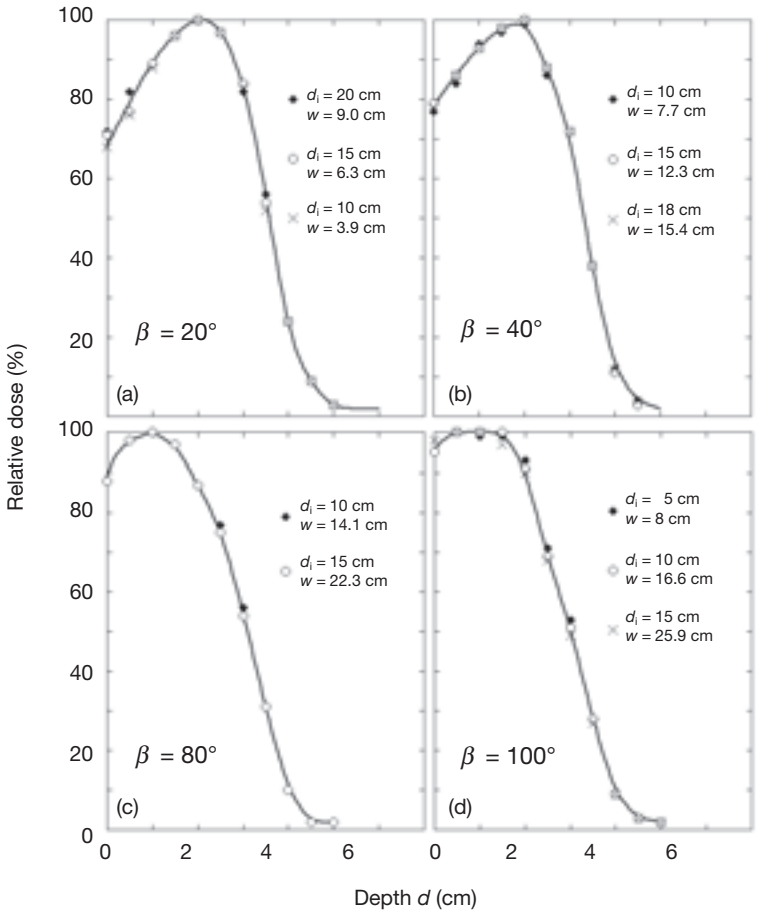

FIG. 8.11. Radial PDDs in electron arc therapy measured in a phantom for various combinations of w and d_i, giving characteristic angles β of (a) 20º, (b) 40º, (c) 80º and (d) 100º. The electron beam energy is 9 MeV.

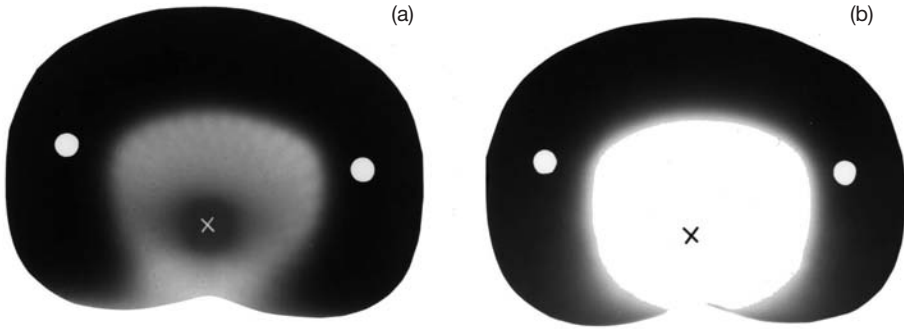

FIG. 8.12. Dose distributions for a 15 MeV rotational electron beam with an isocentre depth d_i of 15 cm, (a) for a β of 10° and (b) for a β of 100°.

One of the technical problems related to electron arc treatment involves the field shape of the moving electron beam defined by secondary collimators. For the treatment of sites that can be approximated with cylindrical geometry (e.g. the chest wall), the field width can be defined by rectangular photon collimators. When treating sites that can only be approximated with a spherical geometry (e.g. the scalp), a custom built secondary collimator defining a non-rectangular field of appropriate shape has to be used to provide a homogeneous dose in the target volume.

8.3.10. Electron therapy treatment planning

The complexity of electron–tissue interactions does not make electron beams well suited to conventional treatment planning algorithms. Electron beams are difficult to model, and look-up table type algorithms do not predict well the dose for oblique incidences or tissue interfaces.

The early methods of electron dose distribution calculations were empirical and based on water phantom measurements of PDDs and beam profiles for various field sizes, similarly to the Milan–Bentley method developed in the late 1960s for use in photon beams. Inhomogeneities were accounted for by scaling the depth dose curves using the CET technique. This technique provides useful parameterization of the electron depth dose curve but has nothing to do with the physics of electron transport, which is dominated by the theory of multiple scattering.

The Fermi–Eyges multiple scattering theory considers a broad electron beam as being made up of many individual pencil beams that spread out laterally in tissue, approximately as a Gaussian function, with the amount of spread increasing with depth. The dose at a particular point in tissue is calculated by an addition of contributions of spreading pencil beams.

The pencil beam algorithm can account for tissue inhomogeneities, patient curvature and irregular field shape. Rudimentary pencil beam algorithms deal with lateral dispersion but ignore angular dispersion and backscattering from tissue interfaces. Subsequent analytical advanced algorithms refined the multiple scattering theory through applying both the stopping powers and the scattering powers but nevertheless generally fail to provide accurate dose distributions in general clinical conditions.

The most accurate way to calculate electron beam dose distributions is through Monte Carlo techniques. The main drawback of the current Monte Carlo approach as a routine dose calculation engine is its relatively long calculation time. However, with ever increasing computer speeds combined with decreasing hardware costs, it can be expected that in the near future Monte Carlo based electron dose calculation algorithms will become available for routine clinical applications.

BIBLIOGRAPHY

INTERNATIONAL ATOMIC ENERGY AGENCY, The Use of Plane Parallel Ionization Chambers in High Energy Electron and Photon Beams, Technical Reports Series No. 381, IAEA, Vienna (1997).

— Absorbed Dose Determination in External Beam Radiotherapy, Technical Reports Series No. 398, IAEA, Vienna (2000).

INTERNATIONAL COMMISSION ON RADIATION UNITS AND MEASUREMENTS, Radiation Dosimetry: Electron Beams with Energies Between 1 and 50 MeV, Rep. 35, ICRU, Bethesda, MD (1984).

JOHNS, H.E., CUNNINGHAM, J.R., The Physics of Radiology, Thomas, Springfield, IL (1985).

KHAN, F.M., The Physics of Radiation Therapy, Lippincott, Williams and Wilkins, Baltimore, MD (2003).

KLEVENHAGEN, S.C., Physics and Dosimetry of Therapy Electron Beams, Medical Physics Publishing, Madison, WI (1993).

VAN DYK, J. (Ed.), Modern Technology of Radiation Oncology: A Compendium for Medical Physicists and Radiation Oncologists, Medical Physics Publishing, Madison, WI (1999).